Chemical Engineering Journal 420 (2021) 130540

Contents lists available at ScienceDirect

Chemical Engineering Journal

journal homepage: www.elsevier.com/locate/cej

Highly hydrophobic polyaniline nanoparticles for anti-corrosion epoxy coatings

Huaiyin Chen [a,b,1], Huizhou Fan [a,1], Nan Su [a], Ruoyu Hong [a,*], Xuesong Lu [c]

[a] College of Chemical Engineering, Fuzhou University, Fuzhou 350108, China
[b] Qingyuan Innovation Laboratory, Quanzhou 362801, China
[c] School of Engineering and Physical Sciences, Heriot-Watt University, Edinburgh EH14 4AS, UK

ARTICLE INFO

Keywords:
Polyaniline
Anti-corrosion coatings
Hydrophobicity
Corrosion inhibition

ABSTRACT

Perfluorooctanoic acid doped polyaniline (PFOA/PANI) nanoparticles were successfully prepared through ultrasonication-assisted oxidation polymerization. The prepared PFOA/PANI nanoparticles exhibited high hydrophobicity and good dispersibility in ethanol, which could uniformly distribute in epoxy resin (EP) coatings to enhance their anti-penetrant efficiency towards corrosive media. The corrosion protection properties of PANI-contained coatings on Q215 steel were evaluated and compared through electrochemical impedance spectroscopy measurements in brine. The experimental results demonstrated the PFOA/PANI/EP coatings possessed higher corrosion performance than the EP coatings and HCl-doped PANI-contained EP coatings. Besides, dedoped PFOA molecules from PFOA/PANI nanoparticles can be adsorbed on the surface of steel to form a hydrophobic corrosion inhibition layer, which further improves the corrosion resistance. The impedance of PFOA/PANI/EP coatings continuously increased after the coatings were immersed in brine for more than 2 days, and the impedance modulus at 0.01 Hz was higher than 6×10^8 Ω·cm^2 after 9 days. The novel method for the preparation of hydrophobic PANI nanoparticles proposed in this work may provide new ideas and methods for developing more high-performance anti-corrosion materials and promoting their applications in corrosion protection.

1. Introduction

Metallic corrosion is a common and irresistible natural phenomenon that seriously damages the engineering equipment, human health and safety, and environment [1]. Therefore, effective anti-corrosion means must be adopted in practical production and life. Organic coatings as a kind of convenient and effective measure, have been extensively used in the field of corrosion protection [2]. However, the barrier effect of pure organic coatings is limited and the coatings will be easily penetrated by corrosive media in a long term. The traditional way to resolve this problem is to add some corrosion inhibition fillers in organic coatings, such as red lead, hexavalent chromium, zinc, and copper. But these corrosion inhibition fillers are toxic, which are harmful to the environment and people's health [3]. Because of that, environmentally friendly and high-efficiency corrosion inhibition fillers are required and pursued.

Polyaniline (PANI) as a classical conducting polymer, has been widely used in various fields, due to its excellent conductivity, redox property, environmental stability, non-toxicity, and facility to modification [4,5]. The corrosion resistance of PANI in coatings or as corrosion inhibitors has been researched for nearly 40 years, since the first report on the PANI-based corrosion inhibition coatings [6]. Lots of studies has proved the effectiveness of polyaniline on corrosion resistance [5,7]. The corrosion resistance performance of PANI coatings is deemed to come from the effects of physical barrier, passivation and corrosion inhibition [8–11]. The difference on the degree of oxidation or protonation would cause the various forms of PANI [8]. Protonated emeraldine is one of the most important forms of PANI that owns electrical conductivity and anti-corrosion property, which can be directly obtained by polymerizing aniline in a solution containing suitable protonic acid [12]. Inorganic acids, such as HCl, H_3PO_4, $HClO_4$, HNO_3, as the most frequently-used doping acids, have been adopted to fabricate various PANI materials [12–14]. However, the inorganic acid-doped PANI materials are difficult to be dissolved or homogeneously dispersed due to the rigid structure of PANI molecules, which seriously limit their

* Corresponding author.
E-mail address: rhong@fzu.edu.cn (R. Hong).
[1] These authors contributed equally to this work.

https://doi.org/10.1016/j.cej.2021.130540
Received 13 December 2020; Received in revised form 30 March 2021; Accepted 22 May 2021
Available online 27 May 2021

applications in coatings and other aspects. Therefore, the organic protonic acids with some functional groups are pursued by more and more researchers in fabrication of doped PANI [15,16]. For example, Chen et al. using partially phosphorylated poly(vinyl alcohol) as the doping acid and modifier prepared conducting PANI nanoparticles that could well dispersed in aqueous media and played an good role in waterborne corrosion protection coatings [9].

The corrosion inhibition has been taken into account by a growing number of researchers in fabricating coatings [17]. The self-healing function to the coatings was sometimes used, thereby further enhancing the performance of corrosion protection in a long term [18–20]. Many organic protonic acids can be adsorbed on the metal surface or integrated with the corrosion products of metal to form dense layers, which generates the corrosion inhibition effect [21]. For example, Hao et al. prepared phytic acid doped PANI and studied its corrosion protection performance and self-healing function in epoxy coatings [22]. They reported that the self-healing function of PANI is ascribed to the synergistic effect of the passivation layer and the complex layer from the combination of the corrosion-produced iron ions and dedoped phytic acid ions. Therefore, it is a promising development direction for the anti-corrosion application of PANI materials that adopting organic protonic acids with corrosion inhibition function to dope PANI in corrosion protection coatings [23]. Though some PANI materials doped with organic protonic acids have been well applied in the corrosion protection coatings, and showed good performances, the hydrophilicity of theses acids doped PANI may accelerate the penetration of water into coatings [24,25]. As known, the water is the essential medium of corrodents, and the high water-resistance of coatings is beneficial to the hinderance towards the penetration of corrosive media [26,27]. Hence the protonic acids with hydrophobic structure are the potential candidate for the doping and modification of PANI with better performance in corrosion resistance.

In this study, adopting perfluorooctanoic acid (PFOA) as the doping acid, highly hydrophobic PANI nanoparticles were facilely synthesized through an ultrasonication-assisted oxidation polymerization method. The PFOA doped PANI (PFOA/PANI) nanoparticles could be homogeneously dispersed in ethanol, which facilitated the homogeneous distribution of PFOA/PANI nanoparticles in epoxy resin (EP) coatings. Due to the high hydrophobicity of and the excellent dispersibility PFOA/PANI nanoparticles, the PFOA/PANI/EP coatings owned good barrier effect towards the penetration of corrosive media. Besides, when PFOA/PANI nanoparticles occur dedoping in coatings, dedoped PFOA molecules can be adsorbed on the surface of steel to form a hydrophobic corrosion inhibition layer, which further improves the corrosion resistance. The synergistic effect of barrier effect, corrosion inhibition and passivation of PFOA/PANI nanoparticles bring about the excellent corrosion resistance of PFOA/PANI/EP coatings. It was innovative that PFOA/PANI nanoparticles with high hydrophobicity, excellent dispersibility and corrosion inhibition were facilely synthesized by using PFOA as the doping acid, and applied to enhancing the corrosion resistance performance of epoxy coatings. We believe this study will give researchers some inspirations to develop more functional materials with wonderful corrosion protection performance and break their application restricts to some extent.

2. Experimental

2.1. Materials

Perfluorooctanoic acid (PFOA) was purchased from Shanghai Adamas Reagent Co., Ltd. Aniline, ammonium persulfate (APS), hexadecyltrimethylammonium chloride (C_{16}TMA), hydrochloric acid and ethanol were purchased from Sinopharm Chemical Reagent Co., Ltd. Aniline was distilled under vacuum prior to use. APS was purified by recrystallization from ethanol. Epoxy (E-44, 6101) and polyamide resin (low molecular weight-650) were purchased from Danbao Resin Co., Ltd. Other chemicals used for this purpose were of analytical grade. The deionized water was used for the preparation of all aqueous solutions.

2.2. Preparation of PFOA/PANI materials

Synthesis process of PFOA/PANI nanoparticles was depicted by Scheme 1(a). Typically, 6.211 g of PFOA (15 mmol), 0.931 g of aniline (10 mmol), 0.064 g of C_{16}TMA, 20 mL of distilled water and 50 mL of ethanol were added into a 250 mL three-necked round-bottom flask to form a homogeneous solution. Then, 30 mL of distilled water solution containing 2.282 g of APS was dropwise added into the as-prepared aqueous solution in an ice bath. After sonicated for 6 h in ice bath, the liquid mixture was stirred at −4 to 0 °C for another 18 h to complete the oxidation polymerization of aniline. Finally, PFOA/PANI nanoparticles were obtained after washing with distilled water and ethanol, and subsequent vacuum drying at 40 °C for 24 h. Besides the PFOA/PANI nanoparticles prepared with the molar ratio of PFOA to aniline of 1.5:1, other PFOA/PANI nanomaterials with the molar ratios of 1:1 and 2:1 were also synthesized, and the corresponding PFOA/PANI nanomaterials were labelled as PFOA/PANI(1.5), PFOA/PANI(1.0) and PFOA/PANI(2.0), respectively. As a contrast, hydrochloric acid-doped PANI (HCl/PANI) nanomaterials were synthesized by the same operation except replacing PFOA with HCl as the doping acid. Note that PFOA/PANI in this paper referred to the PFOA/PANI(1.5), unless the special stated.

2.3. Preparation of PFOA/PANI coatings

The laboratory-made steel electrodes with an exposed area of 1 cm^2 were prepared by mild steel cubes (1 cm^3). Before coatings, the electrodes were polished by sandpaper with different meshes (240, 400, 800, 1000, 1500) and washed with water and ethanol to obtain clean and smooth surfaces. The coatings preparation process is shown in Scheme 1(b). The PFOA/PANI powder was added to the ethanol and ultrasonicated for 1 h to a uniform dispersion. Then the liquid with dispersed PFOA/PANI was poured into the mixture of epoxy resin and polyamide curing agent (weight ratio 3:2), and stirred vigorously using a vertical mill with disk agitator to obtain PFOA/PANI/EP paint, in which the content of PFOA/PANI was 0.75 wt%. Then the paint was spray-coated on the surface of steel samples and dried for 12 h at room temperature followed by air baking in an oven at 60 °C for 24 h to form PFOA/PANI/EP coatings with a thickness of 60 ± 5 μm. Note that the corresponding PFOA/PANI(1.0), PFOA/PANI(1.5) and PFOA/PANI(2.0) contained epoxy coatings were denoted as PFOA/PANI(1.0)/EP coatings, PFOA/PANI(1.5)/EP coatings and PFOA/PANI(2.0)/EP coatings, respectively. The EP coatings, and HCl/PANI/EP coatings were prepared without the addition of PFOA/PANI nanomaterials or replacing them by HCl/PANI nanomaterials.

2.4. Characterization

The morphologies of the synthesized materials were tested by a S-4800 (Hitachi) scanning electron microscope (SEM) and a TECNAI G2 F20 (FEI) transmission electron microscope (TEM). The Avatar 360 (Nicolet) FT-IR spectrometer was adopted to examining the functional groups of the synthesized materials. The measurement of UV–visible spectrum was carried out on a PERSEE TU-1900 spectrophotometer by using a quartz cell with optical path of 10 mm. The structure of the PFOA/PANI nanoparticles was characterized by X-ray diffraction (XRD) through a PANalytical X′Pert Pro X-ray diffractometer using Cu-Kα radiation (40 kV, 40 mA). The surface roughness of PFOA/PANI film surfaces were analyzed by an atomic force microscope (AFM, Bruker Multimode 8). The water contact angle tests of the PFOA/PANI and HCl/PANI films were measured by an automatic contact angle tester (Theta, Attension) with a water droplet of 5 μL. Electrochemical impedance spectroscopy (EIS) was used to investigate the corrosion behavior of

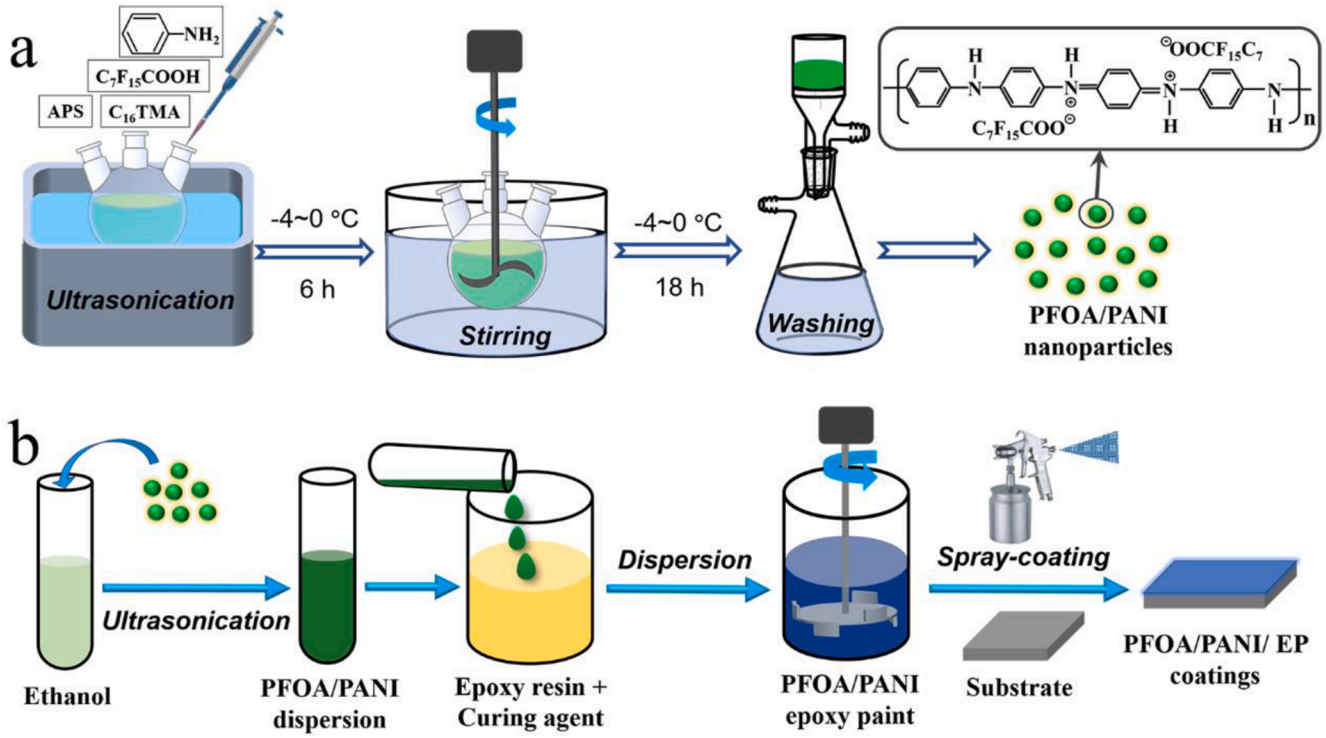

Scheme 1. Schematic of (a) synthesis process of the PFOA/PANI nanoparticles and (b) fabrication process of PFOA/PANI/EP coatings.

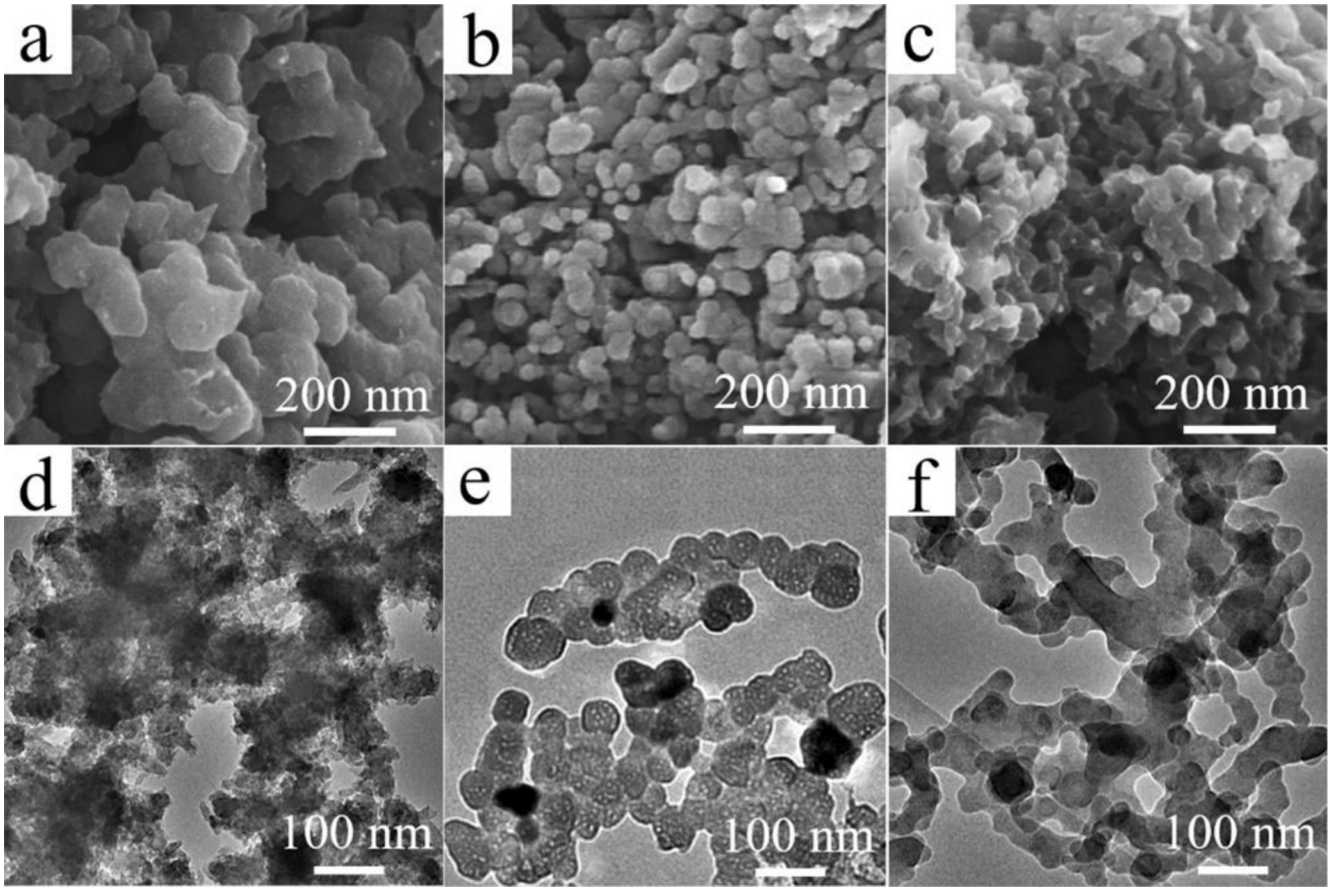

Fig. 1. SEM (a–c) and TEM (d–f) images of PFOA/PANI nanomaterials synthesized with different molar ratio of PFOA to aniline: 1:1 (a, d), 1.5:1 (b, e), and 2:1 (c, f).

steel electrodes in 3.5 wt% NaCl solution at room temperature. EIS tests were performed on an CS165 electrochemical analyzer (Wuhan CorrTest Instruments Corp., Ltd) with a three-electrode system, where the steel electrode as the working electrode, a platinum electrode and a saturated Hg/Hg_2Cl_2 electrode as the counter electrode and the reference electrode, respectively. The frequency range was 100 MHz–0.01 Hz at open circuit potential with the disturbance amplitude of 5 mV.

3. Results and discussion

3.1. Properties of PFOA/PANI nanomaterials

Fig. 1 shows the SEM and TEM images of PFOA/PANI materials, it can be clearly that the prepared PFOA/PANI materials are composed of nano-scale structures. That is because ultrasonic energy at a lower temperature promoted the fracture of growing crystals and led to smaller and relatively uniform crystals compared to the oxidative polymerization without ultrasonic assistance [28]. Fig. 1 also shows that the morphology changes significantly with the molar ratio of PFOA to aniline. When the ratio is 1:1, the SEM image (Fig. 1(a)) shows the PFOA/PANI(1.0) materials are aggregates of irregular particles with the size of 100–180 nm. The aggregate structure of PFOA/PANI(1.0) materials can be confirmed by the TEM image (Fig. 1(d)). As the ratio of PFOA to aniline increases to 1.5:1, the SEM image of PFOA/PANI(1.5) (Fig. 1(b)) shows the particles change to much more uniform and smaller, and the agglomeration phenomenon is relieved. From the TEM image (Fig. 1(e)), it can be found the PFOA/PANI(1.5) particles have the clear profiles and the particle size is about 50–100 nm, corresponding to the result of SEM (Fig. 1(b)). When the ratio further increases to 2:1, the PFOA/PANI(2.0) materials show a porous and cross-linked structure composed of more smaller nanoparticles, as displayed by the SEM image (Fig. 1(c)), and the cross-linked structure can be found more clearly from the TEM image of PFOA/PANI(2.0) materials (Fig. 1(f)). That is because the different acid concentration leads to different polymerization mechanism of aniline, and as a result, the morphology of the obtained PANI changes following the acid concentration [29,30].

Fig. 2 shows the digital photograph of PFOA/PANI nanoparticles and HCl/PANI nanomaterials dispersed in ethanol. For the PFOA/PANI dispersion after 4 days' standing, it looks still uniform and deep-colored, and no sediments are found. On the contrary, the HCl/PANI dispersion shows that there are obvious sediments at the bottom of the sample bottle and hardly any dispersed substances in the dispersion medium. The result indicated that PFOA/PANI nanoparticles had the excellent dispersibility in ethanol, ascribing to the good compatibility between the rigid structure of PANI and the hydrophobic chain of PFOA and good miscibility of PFOA with organic solvent [31]. The excellent dispersibility is conducive to the uniform distribution of PFOA/PANI in EP coatings, thereby slowing down the diffusion rate of corrosive media in the coatings.

FT-IR spectrum of the PFOA/PANI nanoparticles is shown in Fig. 3(a) shows that the characteristic peaks appear at 1582 cm^{-1} (C═C stretching of quinoid rings), 1484 cm^{-1} (C═C stretching of benzenoid rings), 1304 cm^{-1} (C–N stretching of quinoid rings) and 819 cm^{-1} (1,4-substituted phenyl ring stretching), respectively, due to PANI jadeite salt [32]. In addition, the additional peaks at 1233 and 1128 cm^{-1} assign to the symmetric and asymmetric CF_2 stretches [33].

To investigate the structure of PFOA/PANI nanoparticles, the XRD pattern was employed, as displayed in Fig. 3(b). Two intense characteristic peaks appear at about 20.3° and 25.3°, mainly corresponding to the periodicity parallel to the PFOA/PANI polymer chain and the periodic direction perpendicular to the chain direction [34,35], respectively. After doping with PFOA, a part of N atoms in the polymer chain are protonated to produce cations, and a similar "quaternary ammonium salt" with the subsequent "$F_{15}C_8OO$-" is formed. At the same time, the interaction between the molecular chains is also strengthened.

The existence of the emeraldine salt of PFOA/PANI nanoparticles is proved by the UV–Vis spectroscopic measurement of the spheres in ethanol, as shown in Fig. 3(c). The PFOA/PANI nanoparticles show a characteristic peak at 355 nm due to the π–π* transition of benzenoid ring [11]. The absorption peak at 566 nm in PFOA/PANI spectrum is the

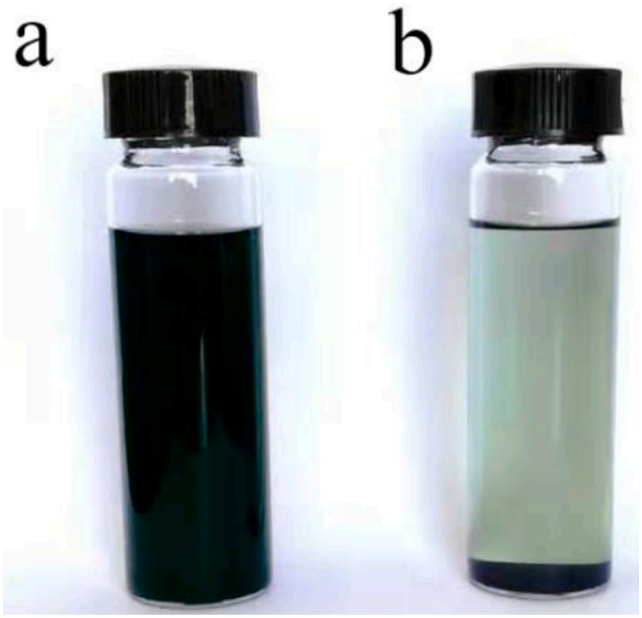

Fig. 2. Digital photograph of PFOA/PANI nanoparticles (a) and HCl/PANI nanomaterials (b) in ethanol after standing for 4 days.

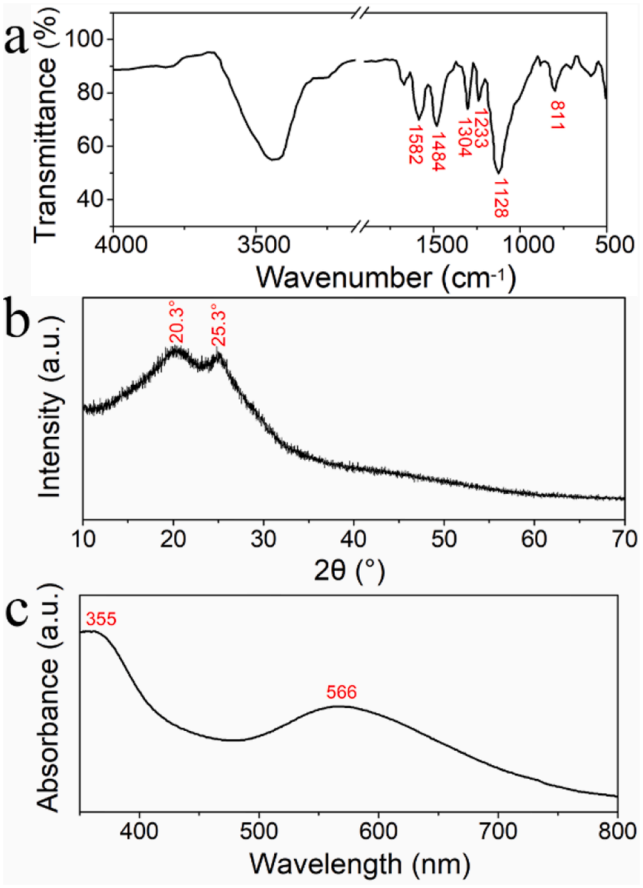

Fig. 3. FT-IR spectrum (a), XRD pattern (b), and UV–vis spectrum (c) of PFOA/PANI nanoparticles.

result of the n–π transition of quinone ring [36]. This test result confirmed the successful synthesis of PFOA/PANI nanoparticles from the structure and composition.

The wettability of prepared materials was tested through the measurements of the water contact angles. Fig. 4 shows the contact angles of the films fabricated by spraying the ethanol dispersion of PFOA/PANI or HCl/PANI nanomaterials. It can be seen clearly that the contact angles of PFOA/PANI nanomaterials are larger than 129°, demonstrating the high hydrophobicity. It is also observed that, the contact angle of PFOA/PANI nanomaterials slightly enlarges from 140.0° to 144.3° with the molar ratio increasing from 1:1 to 1.5:1, and then declines to 129.6 with the molar ratio further increasing to 2:1. The change of contact angle of PFOA/PANI films with the molar ratio of PFOA to aniline is mainly ascribed to their different surface roughness. Fig. 5 shows the AFM morphologies and surface roughness of PFOA/PANI(1.0), PFOA/PANI (1.5) and PFOA/PANI(2.0) films. The film surfaces of PFOA/PANI(2.0), PFOA/PANI(1.0) and PFOA/PANI(1.5) are rougher in sequence, and the corresponding surface roughness (Ra) are 38, 74 and 82 nm, respectively. The AFM results confirm the isotonicity between surface roughness of hydrophobic surface and water contact angle [37]. Fig. 4(d) shows the contact angle of HCl/PANI is about 44.8°, which is much lower than that of PFOA/PANI nanomaterials. The large difference of contact angle between PFOA/PANI and HCl/PANI materials can be explained by Wenzel equation [38]:

$$cos\ \theta_w = r\ (\gamma_{SG} - \gamma_{SL}) / \gamma_{LG} \quad (1)$$

where θ_w, r, γ_{SG}, γ_{SL} and γ_{LG} are apparent contact angle, roughness factor, solid-gas surface tension (solid surface energy), solid-liquid interface tension, and liquid-gas surface tension (liquid surface energy), respectively. Due to the very low surface energy of PFOA, PFOA/PANI nanomaterials also show the small surface tension ($\gamma_{SG,1}$) that much smaller than PFOA/PANI-water interface tension ($\gamma_{SL,1}$). On the contrary, the surface tension of HCl/PANI ($\gamma_{SG,2}$) is much larger HCl/PANI-water interface tension ($\gamma_{SL,2}$). As a result, the apparent contact angles of PFOA/PANI nanomaterials ($\theta_{w,1}$) are much higher than that of HCl/PANI materials ($\theta_{w,2}$), demonstrating PFOA plays an important role in improving the water repellency of PANI. The high hydrophobicity of PFOA/PANI nanoparticles could play a water-resistant barrier role in coatings, which are beneficial for preventing the penetration of corrosive media.

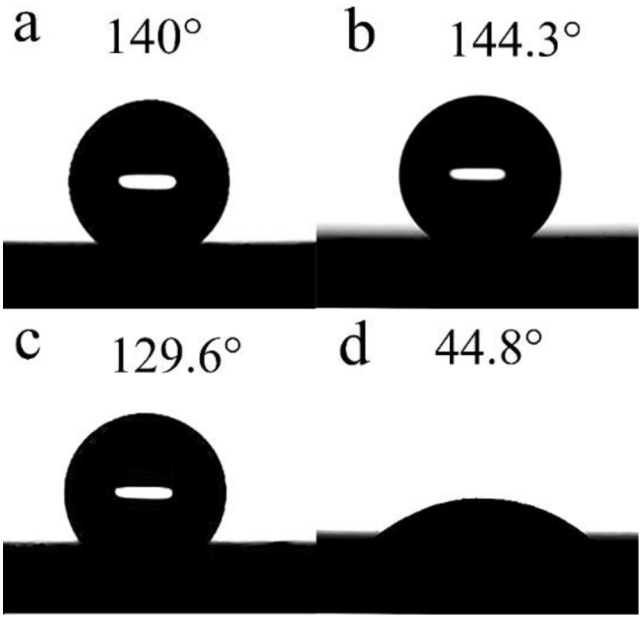

Fig. 4. The water contact angle of PFOA/PANI nanomaterials synthesized with different molar ratio of PFOA to aniline: 1:1 (a), 1.5:1 (b), 2:1 (c), and the water contact angle of HCl/PANI nanomaterials (d).

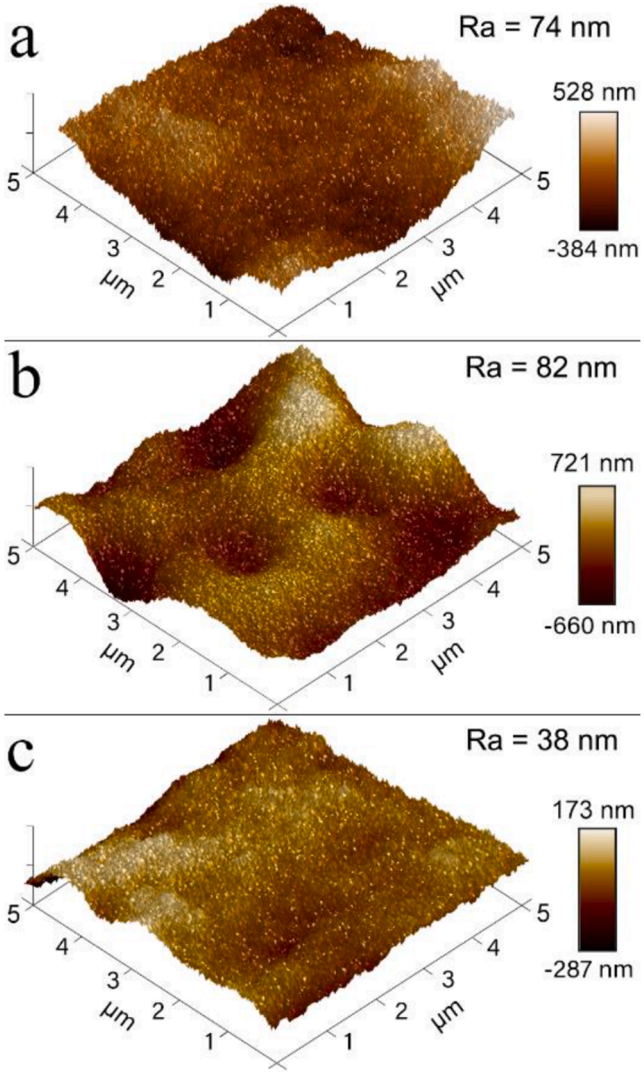

Fig. 5. The AFM morphologies and surface roughness of PFOA/PANI(1.0) film (a), PFOA/PANI(1.5) film (b) and PFOA/PANI(2.0) film (c).

In brief, form the result analysis of dispersity, FT-IR spectrum, XRD pattern, UV–vis spectrum, contact angle and AFM tests, it is proved that PFOA/PANI nanoparticles with high hydrophobicity and excellent dispersibility have been successfully prepared.

3.2. Corrosion resistance of the PFOA/PANI/EP coating

To extend the service lives of metal materials in marine environment, the corrosion resistance of coatings is one of the important metrics. In this study, the corrosion resistances of EP, PFOA/PANI/EP and HCl/PANI/EP coatings were investigated by electrochemical impedance spectroscopy (EIS). The electrochemical corrosion tests of Q215 steel, epoxy resin coated Q215 steel (EP/Q215), PFOA/PANI/EP resin coated Q215 steel (PFOA/PANI/EP/Q215) and HCl/PANI/EP resin coated Q215 steel (HCl/PANI/EP/Q215) were put into 3.5 wt% NaCl solution in order to analyze and compare the corrosion protection performance of each coatings on Q215 steel.

Fig. 6 shows the EIS result of Q215 steel and different coatings. As it is well known, in the same corrosion system, if the diameter of the capacitance loop in the Nyquist plot is larger, the polarization resistance of the working electrode is higher, that is, the corrosion resistance

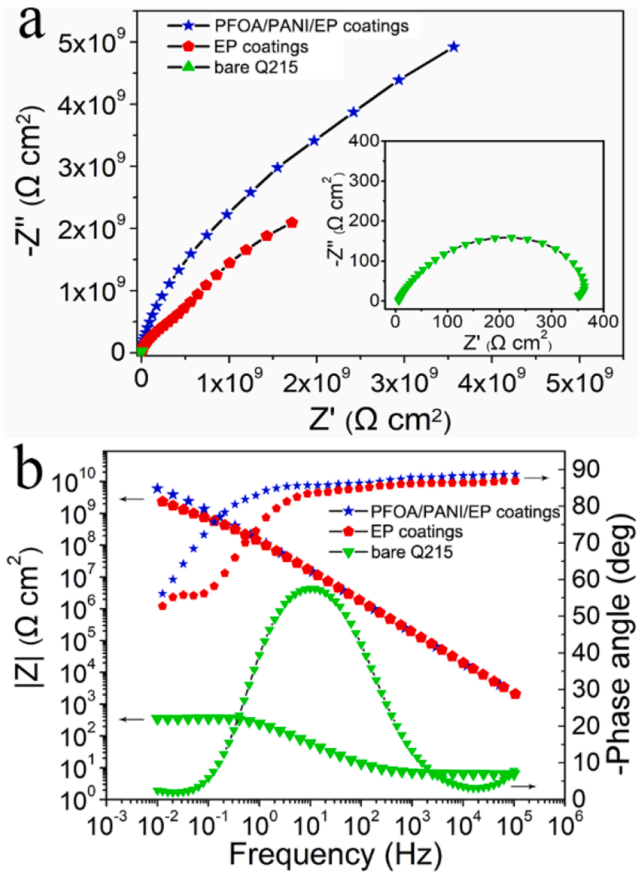

Fig. 6. Nyquist (a) and Bode (b) plots of bare Q215 steel and various coatings after immersion in 3.5 wt% NaCl aqueous solution for 1 h.

performance is better [39,40]. The Nyquist plots (Fig. 6(a)) shows the size relationship of the capacitance loop is PFOA/PANI/EP coatings > EP coatings ≫ bare Q215 steel, indicating the both coatings have good corrosion resistance. Fig. 6(b) depicts the Bode plots present the relationships between impedance modulus |Z| and phase angle versus frequency. It can be seen that the impedance modulus |Z| of the bare Q215 steel is much smaller than that of the EP coatings and PFOA/PANI/EP coatings at the same frequency. The impedance modulus of the coatings at the lower frequency ($|Z|_{0.01\ Hz}$) can be used to evaluate its corrosion resistance [41]. The $|Z|_{0.01\ Hz}$ value shows the trend of PFOA/PANI/EP coatings > EP coatings ≫ bare Q215 steel, and the $|Z|_{0.01\ Hz}$ value of PFOA/PANI/EP coatings is about 7 orders of magnitude greater than that of uncoated Q215 steel, indicating the good corrosion resistance of PFOA/PANI/EP coatings. From the relationship between phase angle and frequency, it is observed that there is an obvious difference between bare Q215 steel and other coatings. The phase angle plot of bare steel shows a sharp peak, which indicates that the electrochemical reaction on Q215 steel is controlled by charge transfer process. However, a very wide half peak can be seen for each coating at medium and high frequency, which indicates that the electrochemical reactions on the coatings are controlled by different electrochemical processes from bare Q215 steel.

In order to further study the effect of different PFOA/PANI nanomaterials on the corrosion resistance of coatings, the corrosion behaviors of the PFOA/PANI/EP coatings prepared from the PFOA/PANI with different molar ratio of PFOA to aniline and HCl/PANI/EP were tested, the experimental results are displayed in Fig. 7. The Nyquist plots of all coatings (Fig. 7(a)) separately display a single-capacity arc with a large and similar arc radius, indicating that all coatings are equivalent to a pure resistance and provide barrier protection. The size of arc value follows the trend of PFOA/PANI (1.5) /EP coatings > PFOA/PANI (1.0)/EP coatings > PFOA/PANI (2.0)/EP coatings > HCl/PANI/EP coatings, indicating PFOA/PANI (1.5)/EP coatings plays the best barrier effect. It may be due to the better hydrophobicity of PFOA/PANI (1.5)/EP nanomaterial. The Bode plots of (Fig. 7(b, c)) show that all the coatings

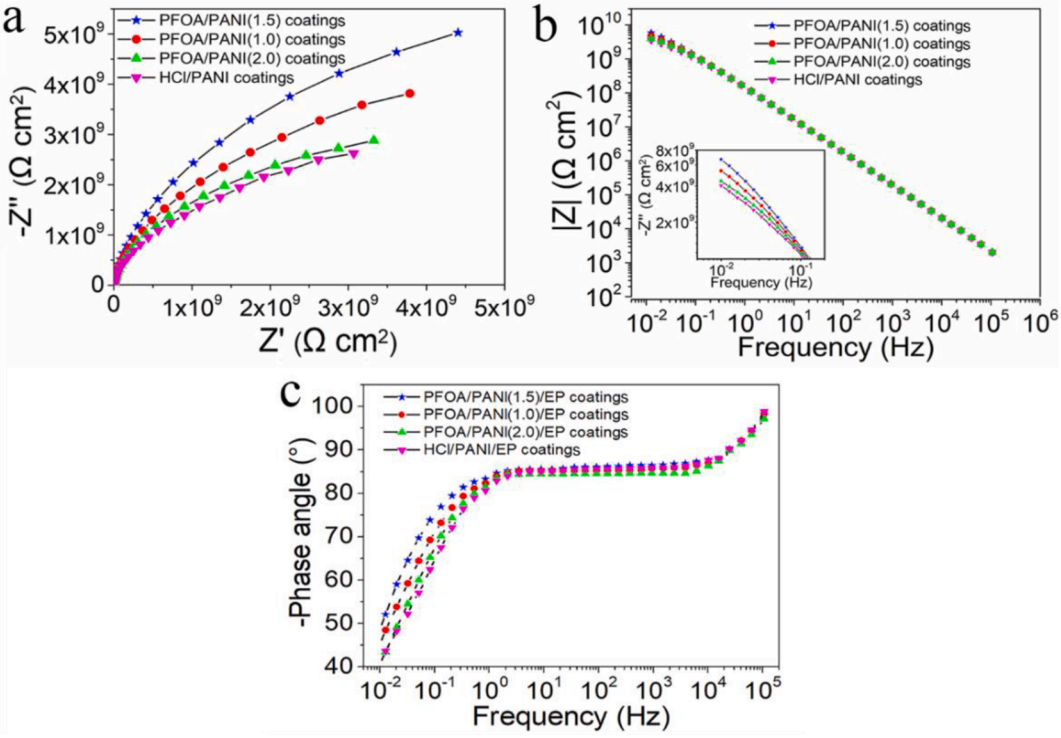

Fig. 7. Nyquist plot (a) and Bode plots of impedance modulus versus frequency (b) and phase angle versus frequency (c) of different coatings after immersed in 3.5 wt% NaCl aqueous solution for 1 h.

display the concurrent trend in impedance modulus |Z| and phase angle, demonstrating the similar electrochemical processes and protection behavior at the initial stage. It can also be observed that the $|Z|_{0.01\ Hz}$ value of the PFOA/PANI (1.5)/EP coatings is the largest, which is corresponds to the result of Nyquist plot.

In order to investigate the long-term protection effect of EP coatings, PFOA/PANI/EP coatings and HCl/PANI/EP coatings were tested by immersion in 3.5 wt% NaCl aqueous solution for different period. Fig. 8 shows the changes of Nyquist and $|Z|_{0.01\ Hz}$ with the immersion time. The Nyquist plot of EP coatings (Fig. 8(a)) shows that capacitive loop is two rings after 0.5 day of immersion, and the radius of the arc decreases rapidly with the increase of immersion time, which indicates corrosive medium has permeated the EP coatings and the steel is partly corroded. As shown in Fig. 8(b), the $|Z|_{0.01\ Hz}$ value of EP coatings quickly dropped from $1.03 \times 10^7\ \Omega{\cdot}cm^2$ (0.5 day) to $7.01 \times 10^5\ \Omega{\cdot}cm^2$ (5 days), indicating the anti-corrosion performance of the coatings is greatly reduced. This result proves that the EP coatings are flimsy and have no long-term effective corrosion resistance. The Nyquist curve of the PFOA/PANI/EP coatings (Fig. 8(c)) depicts a different variation trend of capacitive loop with that of EP coatings. After the soaking for 0.5–2 days, the Nyquist curves of the PFOA/PANI/EP coatings are composed of a semicircular capacitive loop and a straight line, and the capacitive loop decreases gradually with the increase of soaking time. The presence of straight line represents that the reaction process controlled by the mass transfer of corrosion products. The capacitive loop decreases to the minimum value after 2 days' immersion, and then increases with the further increase of immersion time, indicating that a dense passivation film is generated on steel surface. Fig. 8(d) shows that the $|Z|_{0.01\ Hz}$ value of PFOA/PANI/EP coatings decreases slowly from 7.88×10^8 to $4.53 \times 10^8\ \Omega{\cdot}cm^2$ within in 2 days, and then increases slowly to $6.76 \times 10^8\ \Omega{\cdot}cm^2$. This result shows that the PFOA/PANI/EP coatings have a high-efficiency barrier effect and corrosion inhibition effect. For HCl/PANI/EP coatings, the radius of the arc displays a trend of decrease-increase-decrease (Fig. 8(e)). The $|Z|_{0.01\ Hz}$ of HCl/PANI coatings decreases sharply from 5.52×10^8 to $1.20 \times 10^8\ \Omega{\cdot}cm^2$ after immersion for 3 days, and increases to $3.54 \times 10^8\ \Omega{\cdot}cm^2$ when the immersion time further is extended to 6 days, and then decreases again to $1.98 \times 10^7\ \Omega{\cdot}cm^2$ after 9 days (Fig. 8(f)). It may be because HCl/PANI possess a short-time passivation effect. The EIS results of those coatings confirm that this novel PFOA/PANI nanoparticles have the best corrosion protection performance.

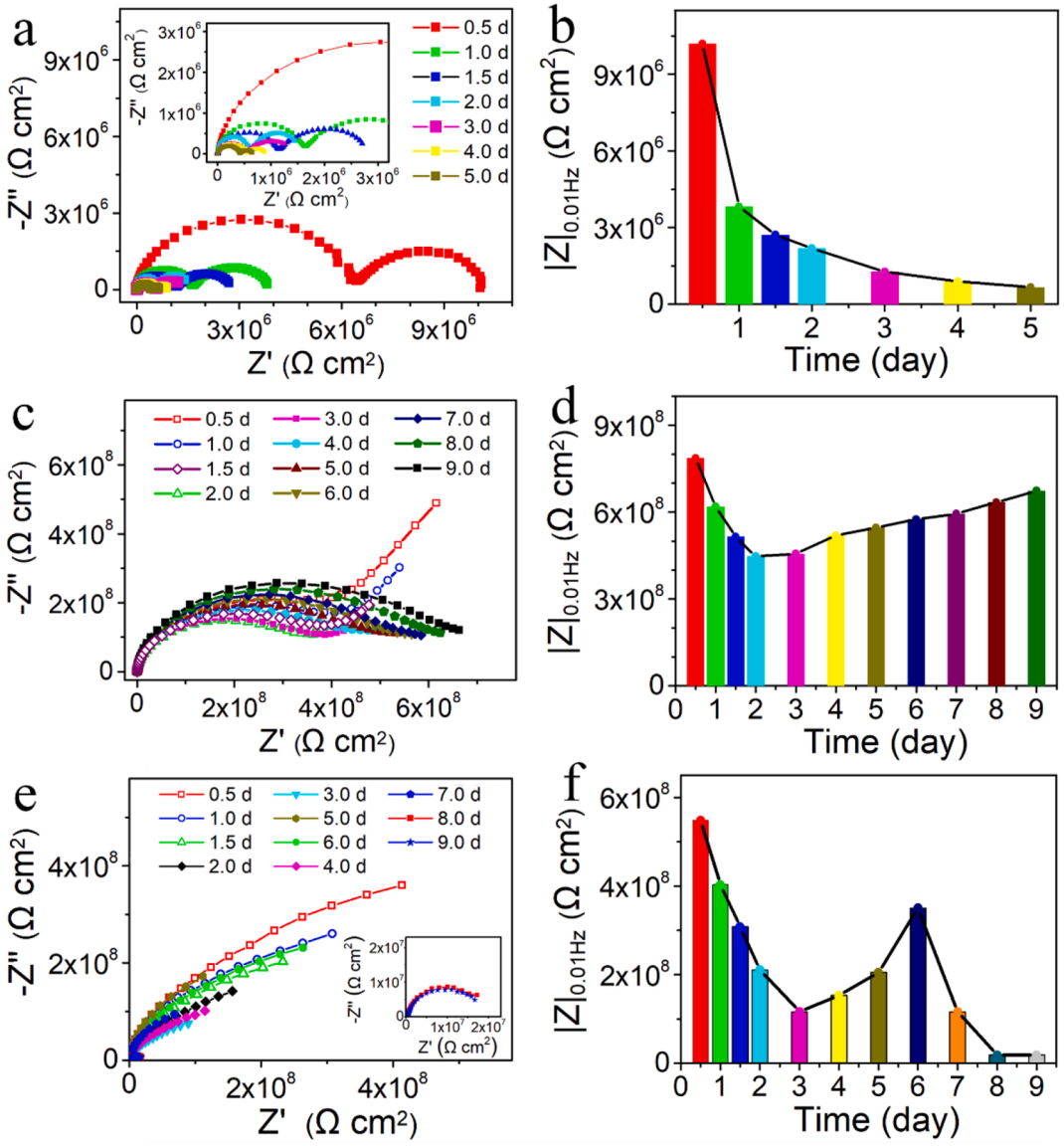

Fig. 8. The Nyquist plots (a, c, e) and the change plots of $|Z|_{0.01\ Hz}$ values (b, d, f) of EP coatings (a, b), PFOA/PANI/EP coatings (c, d) and HCl/PANI/EP coatings (e, f) on Q215 steel with different immersion times in 3.5 wt% NaCl aqueous solution.

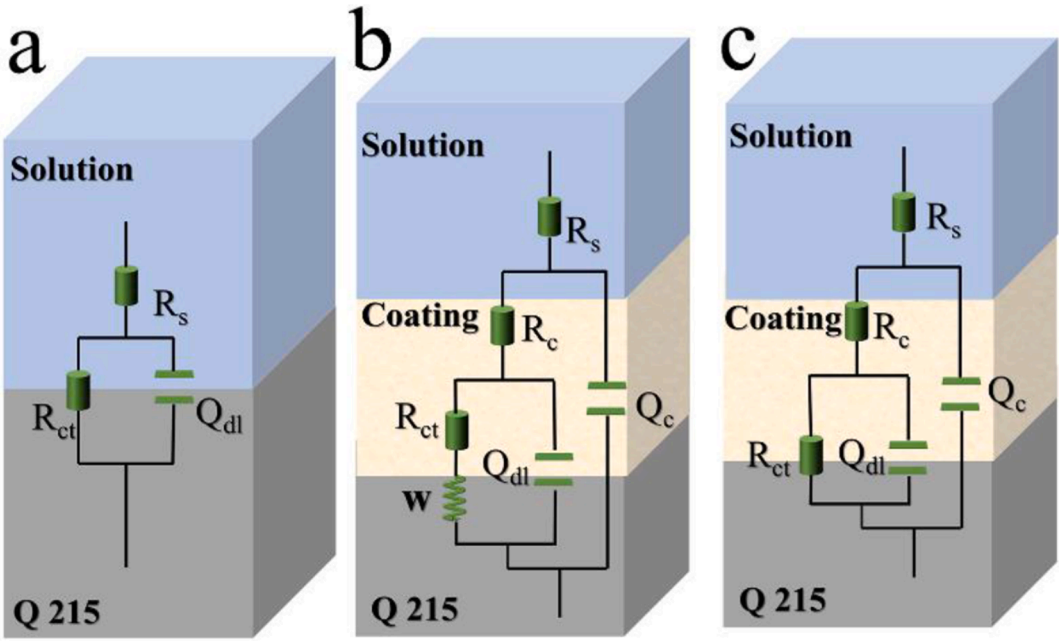

Fig. 9. The electrical equivalent circuit models used for bare Q215 steel (a), the initial stage (b) and later stage (c) of PFOA/PANI/EP coatings in 3.5 wt% NaCl aqueous solution.

Fig. 9 exhibits the equivalent circuit graphics of Q215 electrode and PFOA/PANI/EP coatings in 3.5 wt% NaCl aqueous solution, where R_s, R_{ct}, R_c, Q_c, Q_{dl} and W represent solution resistance, charge transfer resistance, coating resistance, constant phase angle element correlating with coating capacitance, constant phase angle element correlating with double layer capacitance, and Warburg impedance, respectively. Fig. 9 (a) shows the equivalent circuit model of bare Q215 steel, consisting of solution resistance (R_s), constant phase angle element correlating with double layer capacitance (Q_{dl}) and charge transfer resistance (R_{ct}). The second model (Fig. 9(b)) is suitable for PFOA/PANI/EP coatings immersed 3.5 wt% NaCl solution less than 2 days. Due to the permeation of corrosive medium into the coatings, the metal was corroded, and the diffusion of corrosion products became a controlling process. Therefore, the equivalent circuit is composed of solution resistance (R_s), coating resistance (R_c), constant phase angle element correlating with coating capacitance (Q_c), charge transfer resistance (R_{ct}), constant phase angle element correlating with double layer capacitance (Q_{dl}), and Warburg impedance (W). Different from the model in Fig. 9(b), there is no Warburg impedance (W) element in the equivalent circuit model depicted by Fig. 9(c)), which is suitable for PFOA/PANI/EP coatings with the immersion time more than 2 days. Due to the corrosion inhibition of PFOA/PANI nanoparticles, the corrosion resistance was enhanced, and the corrosion rate was slowed down, as a result, the diffusion process of corrosion products became negligible. The results demonstrate that the PFOA/PANI/EP coatings have a durable corrosion resistance.

Table 1 shows the equivalent circuit fitting results of Q215 bare steel and PFOA/PANI/EP coatings. It can be seen that the charge transfer resistance (R_{ct}) of the PFOA/PANI/EP coatings in 3.5 wt% NaCl solution for 1 day reaches 3.62×10^8 Ω·cm^2. After 9 days, the charge transfer resistance (R_{ct}) increased to 5.25×10^8 Ω·cm^2, demonstrating the excellent corrosion inhibition of PFOA/PANI/EP coatings. Furthermore, the charge transfer resistance of the PFOA/PANI/EP coatings is 7 orders of magnitudes higher than that of bare Q215 steel, which indicates the coatings has an effective corrosion resistance.

3.3. Anticorrosion mechanism of the PFOA/PANI/EP coating

The anti-corrosion effect of the PFOA/PANI/EP coatings on steel surface is mainly ascribed to the following factors: the barrier effect, passivation effect and corrosion inhibition of PFOA/PANI nanoparticles in EP coating, as described by Fig. 10. Due to the high water-resistance of and good compatibility with epoxy resin, PFOA/PANI nanomaterials as filler can fill up the pores of the coatings, and hold back the corrosive media to reach the metal substrate [42]. The passivation effect is offered by the formation of Fe_2O_3 layer due to the redox reaction between different structure forms of PFOA/PANI [43–45]. Besides, PFOA molecule has a hydrophilic carboxyl group and a hydrophobic long chain, which can be adsorbed on the surface of metal to form a hydrophobic film. In the process of application, PFOA molecule can dedope from PFOA/PANI [46], and form a hydrophobic corrosion inhibition layer on the surface of metal to further enhance the corrosion resistance of the coatings [24].

4. Conclusions

In this work, using PFOA as the dopant, PFOA/PANI nanoparticles

Table 1
Electrochemical parameters of EIS measurements fitted though proper electrical equivalent circuits.

Sample*	R_s (Ω cm^2)	Q_c		R_c (Ω cm^2)	Q_{dl}		R_{ct} (Ω cm^2)	W
		Y_0 (F cm^{-2})	n		Y_0 (F cm^{-2})	n		
a	6.52	\	\	\	6.25×10^{-4}	0.79	38.47	\
b	4.58	2.00×10^{-10}	0.62	3.23×10^8	1.09×10^{-9}	0.97	3.62×10^8	1.15×10^{-8}
c	5.86	1.16×10^{-9}	0.96	3.71×10^8	3.68×10^{-9}	0.37	5.25×10^8	\

* Sample a denoted the bare Q215; sample b and c denoted the PFOA/PANI/EP coatings after immersion in 3.5 wt% NaCl aqueous solution for 1 day and 9 days, respectively.

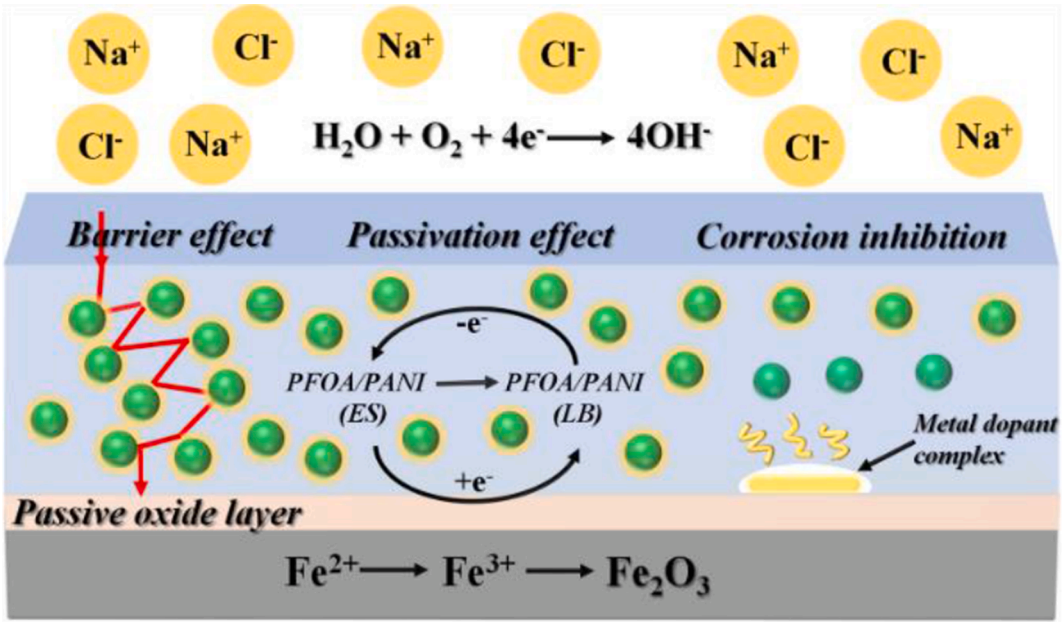

Fig. 10. Scheme of anticorrosion mechanism of PFOA/PANI/EP coatings on Q215 steel surface.

were synthesized by the chemical oxidative polymerization of aniline. The PFAO/PANI nanoparticles displayed high hydrophobicity and excellent dispersibility in ethanol, which is beneficial for the uniform distribution in epoxy resin. The PFAO/PANI/EP coatings were facilely prepared by spraying and applied to the research of anti-corrosion performance for Q215 steel. The corrosion protection properties of the coatings were evaluated and compared through EIS measurements in the 3.5 wt% NaCl solution. The result shows that PFOA/PANI/EP coatings with the higher corrosion performance than the EP coatings and HCl/PANI/EP coatings. The $|Z|_{0.01\ Hz}$ value of PFOA/PANI/EP coatings continuously increases after the coatings were immersed in the 3.5 wt% NaCl solution for more than 2 days, demonstrating that the corrosion protection performance was enhanced. The corrosion protection mechanisms of PFOA/PANI/EP coatings are ascribed to the efficient physical barrier effect, passivation effect and corrosion inhibition of PFOA/PANI nanoparticles in EP coatings. The novel method for preparation of hydrophobic PANI this paper proposed proved new ideas and methods for developing more efficient and multifunctional anticorrosive materials.

Declaration of Competing Interest

The authors declare that they have no known competing financial interests or personal relationships that could have appeared to influence the work reported in this paper.

Acknowledgments

This work was supported by Fuzhou University Testing Fund of precious apparatus (Nos. 2021T023, 2020T025), Minjiang Scholarship of Fujian Province (No. Min-Gaojiao [2010]-117), Central Government Guiding Special funds for Local Science and Technology Development (No. 830170778), R&D Fund for Strategic Emerging Industry of Fujian Province (No. 82918001), and International Cooperation Project of Fujian Science and Technology Department (No. 830170771).

References

[1] B. Hou, X. Li, X. Ma, C. Du, D. Zhang, M. Zheng, W. Xu, D. Lu, F. Ma, The cost of corrosion in China, NPJ Mater. Degrad. 1 (2017) 4.
[2] R. Guo, J. Wang, H. Wang, G. Fei, C. Wang, L. Sun, G.G. Wallace, Engineering the poly(vinyl alcohol)-polyaniline colloids for high-performance waterborne alkyd anticorrosion coating, Appl. Surf. Sci. 481 (2019) 960–971.
[3] S. Qiu, C. Chen, M. Cui, W. Li, H. Zhao, L. Wang, Corrosion protection performance of waterborne epoxy coatings containing self-doped polyaniline nanofiber, Appl. Surf. Sci. 407 (2017) 213–222.
[4] X. Zhu, Z. Ni, L. Dong, Z. Yang, L. Cheng, X. Zhou, Y. Xing, J. Wen, M. Chen, In-situ modulation of interactions between polyaniline and graphene oxide films to develop waterborne epoxy anticorrosion coatings, Prog. Org. Coat. 133 (2019) 106–116.
[5] C. Yang, H. Wei, L. Guan, J. Guo, Y. Wang, X. Yan, X. Zhang, S. Wei, Z. Guo, Polymer nanocomposites for energy storage, energy saving, and anticorrosion, J. Mater. Chem. A 3 (2015) 14929–14941.
[6] G. Mengoli, M.T. Munari, P. Bianco, M.M. Musiani, Anodic synthesis of polyaniline coatings onto Fe sheets, J. Appl. Polym. Sci. 26 (1981) 4247–4257.
[7] M. Rohwerder, A. Michalik, Conducting polymers for corrosion protection: what makes the difference between failure and success? Electrochim. Acta 53 (2007) 1300–1313.
[8] A. Kalendová, I. Sapurina, J. Stejskal, D. Veselý, Anticorrosion properties of polyaniline-coated pigments in organic coatings, Corros. Sci. 50 (2008) 3549–3560.
[9] F. Chen, P. Liu, Conducting polyaniline nanoparticles and their dispersion for waterborne corrosion protection coatings, ACS Appl. Mater. Interfaces 3 (2011) 2694–2702.
[10] Y. Luo, Y. Sun, J. Lv, X. Wang, J. Li, F. Wang, Transition of interface oxide layer from porous $Mg(OH)_2$ to dense MgO induced by polyaniline and corrosion resistance of Mg alloy therefrom, Appl. Surf. Sci. 328 (2015) 247–254.
[11] Y. Hayatgheib, B. Ramezanzadeh, P. Kardar, M. Mahdavian, A comparative study on fabrication of a highly effective corrosion protective system based on graphene oxide-polyaniline nanofibers/epoxy composite, Corros. Sci. 133 (2018) 358–373.
[12] Y. Zhang, Y. Shao, T. Zhang, G. Meng, F. Wang, The effect of epoxy coating containing emeraldine base and hydrofluoric acid doped polyaniline on the corrosion protection of AZ91D magnesium alloy, Corros. Sci. 53 (2011) 3747–3755.
[13] S. Sathiyanarayanan, S. Muthkrishnan, G. Venkatachari, Corrosion protection of steel by polyaniline blended coating, Electrochim. Acta 51 (2006) 6313–6319.
[14] G. Ebrahimi, J. Neshati, F. Rezaei, An investigation on the effect of H_3PO_4 and HCl-doped polyaniline nanoparticles on corrosion protection of carbon steel by means of scanning kelvin probe, Prog. Org. Coat. 105 (2017) 1–8.
[15] C. Zhou, M. Hong, Y. Yang, N. Hu, Z. Zhou, L. Zhang, Y. Zhang, Engineering sulfonated polyaniline molecules on reduced graphene oxide nanosheets for high-performance corrosion protective coatings, Appl. Surf. Sci. 484 (2019) 663–675.
[16] S. Liu, L. Liu, X. Wei, B. Zhang, F. Meng, F. Wang, Oxide film formed on Al alloy beneath sulfosalicylic acid doped polyaniline incorporated into epoxy organic coating, Appl. Surf. Sci. 512 (2020), 144840.
[17] J. Wen, J. Lei, J. Chen, J. Gou, Y. Li, L. Li, An intelligent coating based on pH-sensitive hybrid hydrogel for corrosion protection of mild steel, Chem. Eng. J. 392 (2020), 123742.
[18] J. Cui, X. Li, Z. Pei, Y. Pei, A long-term stable and environmental friendly self-healing coating with polyaniline/sodium alginate microcapsule structure for corrosion protection of water-delivery pipelines, Chem. Eng. J. 358 (2019) 379–388.
[19] Y. Hao, Y. Zhao, X. Yang, B. Hu, S. Ye, L. Song, R. Li, Self-healing epoxy coating loaded with phytic acid doped polyaniline nanofibers impregnated with benzotriazole for Q235 carbon steel, Corros. Sci. 151 (2019) 175–189.

[20] N. Pirhady Tavandashti, M. Ghorbani, A. Shojaei, J.M.C. Mol, H. Terryn, K. Baert, Y. Gonzalez-Garcia, Inhibitor-loaded conducting polymer capsules for active corrosion protection of coating defects, Corros. Sci. 112 (2016) 138–149.
[21] Y. Ma, B. Fan, H. Liu, G. Fan, H. Hao, B. Yang, Enhanced corrosion inhibition of aniline derivatives electropolymerized coatings on copper: preparation, characterization and mechanism modeling, Appl. Surf. Sci. 514 (2020), 146086.
[22] Y. Hao, L.A. Sani, T. Ge, Q. Fang, Phytic acid doped polyaniline containing epoxy coatings for corrosion protection of Q235 carbon steel, Appl. Surf. Sci. 419 (2017) 826–837.
[23] B. Ramezanzadeh, G. Bahlakeh, M. Ramezanzadeh, Polyaniline-cerium oxide (PAni-CeO_2) coated graphene oxide for enhancement of epoxy coating corrosion protection performance on mild steel Check, Corros. Sci. 137 (2018) 111–126.
[24] G. Gupta, N. Birbilis, A.B. Cook, A.S. Khanna, Polyaniline-lignosulfonate/epoxy coating for corrosion protection of AA2024-T3, Corros. Sci. 67 (2013) 256–267.
[25] M. Cui, S. Ren, H. Zhao, Q. Xue, L. Wang, Polydopamine coated graphene oxide for anticorrosive reinforcement of water-borne epoxy coating, Chem. Eng. J. 335 (2018) 255–266.
[26] Y. Li, X. Zhang, Y. Cui, H. Wang, J. Wang, Anti-corrosion enhancement of superhydrophobic coating utilizing oxygen vacancy modified potassium titanate whisker, Chem. Eng. J. 374 (2019) 1326–1336.
[27] R. Yuan, H. Liu, Y. Chen, Z. Liu, Z. Li, J. Wang, G. Jing, Y. Zhu, P. Yu, H. Wang, Design ambient-curable superhydrophobic/electroactive coating toward durable pitting corrosion resistance, Chem. Eng. J. 374 (2019) 840–851.
[28] H. Kafashan, M. Azizieh, H. Nasiri Vatan, Ultrasound-assisted electrodeposition of SnS: effect of ultrasound waves on the physical properties of nanostructured SnS thin films, J. Alloy. Compd. 686 (2016) 962–968.
[29] J.-C. Chiang, A.G. MacDiarmid, 'Polyaniline': Protonic acid doping of the emeraldine form to the metallic regime, Synth. Met. 13 (1986) 193–205.
[30] D. Banerjee, A.K. Kar, Influence of polaron doping and concentration dependent FRET on luminescence of PAni–PMMA blends for application in PLEDs, Phys. Chem. Chem. Phys. 20 (2018) 23055–23071.
[31] R. Yuan, H. Wang, T. Ji, L. Mu, L. Chen, Y. Zhu, J. Zhu, Superhydrophobic polyaniline hollow spheres with mesoporous brain-like convex-fold shell textures, J. Mater. Chem. A 3 (2015) 19299–19303.
[32] Y. Zhu, D. Hu, M.X. Wan, L. Jiang, Y. Wei, Conducting and superhydrophobic Rambutan-like hollow spheres of polyaniline, Adv. Mater. 19 (2007) 2092–2096.
[33] K.K.S. Lau, S.K. Murthy, H.G.P. Lewis, J.A. Caulfield, K.K. Gleason, Fluorocarbon dielectrics via hot filament chemical vapor deposition, J. Fluorine Chem. 122 (2003) 93–96.
[34] J.P. Pouget, M.E. Jozefowicz, A.J. Epstein, X. Tang, A.G. MacDiarmid, X-ray structure of polyaniline, Macromolecules 24 (1991) 779–789.
[35] D. Chao, X. Lu, J. Chen, X. Liu, W. Zhang, Y. Wei, Synthesis and characterization of electroactive polyamide with amine-capped aniline pentamer and ferrocene in the main chain by oxidative coupling polymerization, Polymer 47 (2006) 2643–2648.
[36] P.T. Bertuoli, A.F. Baldissera, A.J. Zattera, C.A. Ferreira, C. Alemán, E. Armelin, Polyaniline coated core-shell polyacrylates: control of film formation and coating application for corrosion protection, Prog. Org. Coat. 128 (2019) 40–51.
[37] Y. Si, Z. Guo, Superhydrophobic nanocoatings: from materials to fabrications and to applications, Nanoscale 7 (2015) 5922–5946.
[38] R.N. Wenzel, Resistance of solid surfaces to wetting by water, Ind. Eng. Chem. 28 (1936) 988–994.
[39] Z. She, Q. Li, Z. Wang, L. Li, F. Chen, J. Zhou, Researching the fabrication of anticorrosion superhydrophobic surface on magnesium alloy and its mechanical stability and durability, Chem. Eng. J. 228 (2013) 415–424.
[40] H. Chen, F. Wang, H. Fan, R. Hong, W. Li, Construction of MOF-based superhydrophobic composite coating with excellent abrasion resistance and durability for self-cleaning, corrosion resistance, anti-icing, and loading-increasing research, Chem. Eng. J. 408 (2021), 127343.
[41] Y. Ye, Z. Liu, W. Liu, D. Zhang, H. Zhao, L. Wang, X. Li, Superhydrophobic oligoaniline-containing electroactive silica coating as pre-process coating for corrosion protection of carbon steel, Chem. Eng. J. 348 (2018) 940–951.
[42] Y. Situ, W. Ji, C. Liu, J. Xu, H. Huang, Synergistic effect of homogeneously dispersed PANI-TiN nanocomposites towards long-term anticorrosive performance of epoxy coatings, Prog. Org. Coat. 130 (2019) 158–167.
[43] S.R. Moraes, D. Huerta-Vilca, A.J. Motheo, Corrosion protection of stainless steel by polyaniline electrosynthesized from phosphate buffer solutions, Prog. Org. Coat. 48 (2003) 28–33.
[44] I. Šeděnková, J. Prokeš, M. Trchová, J. Stejskal, Conformational transition in polyaniline films – spectroscopic and conductivity studies of ageing, Polym. Degrad. Stab. 93 (2008) 428–435.
[45] P.J. Kinlen, Y. Ding, D.C. Silverman, Corrosion protection of mild steel using sulfonic and phosphonic acid-doped polyanilines, Corrosion 58 (2002) 490–497.
[46] X. Zhou, Z. Zhang, X. Men, J. Yang, X. Xu, X. Zhu, Q. Xue, Fabrication of superhydrophobic polyaniline films with rapidly switchable wettability, Appl. Surf. Sci. 258 (2011) 285–289.